Chemical Science

ROYAL SOCIETY OF CHEMISTRY

EDGE ARTICLE

View Article Online
View Journal | View Issue

Cite this: *Chem. Sci.*, 2022, **13**, 531

All publication charges for this article have been paid for by the Royal Society of Chemistry

Received 5th November 2021
Accepted 13th December 2021

DOI: 10.1039/d1sc06154b

rsc.li/chemical-science

Sequence-independent activation of photocycloadditions using two colours of light†

Philipp W. Kamm,[abc] Leona L. Rodrigues,[ab] Sarah L. Walden,[ab] James P. Blinco, *[ab] Andreas-Neil Unterreiner *[c] and Christopher Barner-Kowollik *[ab]

We exploit two reactive chromophores to establish sequence-independent photochemical activation, employing *ortho*-methyl benzaldehyde (**o**MBA) and *N*,*N*-(dimethylamino)pyrene aryl tetrazole (**APAT**) with *N*-(2-hydroxy)ethyl maleimide (**NHEM**), without any additives. Critically, the order of the irradiation sequence is irrelevant, as the shorter wavelength does not activate the higher wavelength activated species. Therefore, full sequence-independent λ-orthogonality is achieved through differences in both the reaction quantum yields ($\Phi_{r,oMBA}$ and $\Phi_{r,APAT}$) and wavelength-dependent reactivity profiles of the employed chromophores.

Introduction

Spatio-temporal resolution, energy efficiency and innocuousness are hallmarks of photochemistry.[1–5] By manipulating the wavelength and intensity of light, chemists are moving towards precise control over multi-component reaction systems.[6,7] Independently addressing specific photoreactive moieties alongside each other is called λ-orthogonality,[8] wavelength selectivity,[9,10] or chromatic orthogonality.[11] In recent years, λ-orthogonal systems have gained interest because their one-pot nature offers simplicity over conventional multi-step protection-group chemistry, while maintaining modularity.[12] This is demonstrated by a multitude of applications such as advanced synthetic protocols,[13–15] post-functionalisation of polymers,[16] or tuning of material properties.[17] Attaining full λ-orthogonality, however, is a challenging endeavour. It requires exclusively addressing one photo-active site and reaching high conversions, while the other component remains unaffected, and *vice versa*. This is mostly achieved through designing red-shifted chromophores with distinct absorption spectra.[17,18] Yet even red-shifted chromophores usually display significant absorption in the short-wavelength region. Thus, spectral overlap in multi-component arrays is often unavoidable, and irradiation at shorter wavelengths usually triggers both photo-active units.[8] The lack of spectral disparity therefore necessitates irradiation with different colours of light in a predefined sequence. Thus, low-energy light is applied first until complete conversion of the long-wavelength selective moiety is achieved, followed by high-energy light to convert the short-wavelength selective moiety.[19–23] Exceptions to this constraint mostly involve photocleavable protecting groups or uncaging units,[24–26] however examples of fully sequence-independent λ-orthogonal systems for covalent bond formation remain scarce.

Two common types of visible or UV light-activated covalent bond forming reactions are the nitrile imine-mediated tetrazole-ene cycloaddition (NITEC) and the *o*-quinodimethane-mediated Diels–Alder reaction of *o*-methylbenzaldehydes (*o*MBA). Upon irradiation with visible or UV light, tetrazoles eject molecular nitrogen, forming a highly reactive nitrile imine intermediate that can react with a range of substitutes.[27] Upon UV irradiation, *ortho*-methylbenzaldehydes undergo photoisomerization, generating hydroxy-*o*-quinodimethanes that are able to perform Diels–Alder cycloadditions with electron-deficient enes. Our group recently introduced a combination of 2,5-diphenyltetrazole and *o*MBA thioether for sequence-independent ligation with 285 nm and 382 nm light.[28] In the presence of water, the reaction quantum yield of the latter is significantly lowered and irradiation with 285 nm light therefore exclusively leads to conversion of the tetrazole, meaning that sequence-independence is achieved through switching solvents prior to changing the colour of light. Reducing this preparative complexity is a matter of priority.

When designing a λ-orthogonal reaction system, not only absorption spectra, but also reaction quantum yields must be taken into account.[29] This is especially relevant since the wavelength-dependent reactivity often deviates from the absorption profiles of the respective chromophores.[30,31] To

[a]*Centre for Materials Science, Queensland University of Technology (QUT), 2 George Street, Brisbane, QLD 4000, Australia. E-mail: j.blinco@qut.edu.au; christopher.barnerkowollik@qut.edu.au*

[b]*School of Chemistry and Physics, Queensland University of Technology (QUT), 2 George Street, Brisbane, QLD 4000, Australia*

[c]*Molecular Physical Chemistry Group, Institute of Physical Chemistry, Karlsruhe Institute of Technology (KIT), Fritz-Haber-Weg 2, Geb. 30.44, Karlsruhe 76131, Germany. E-mail: andreas.unterreiner@kit.edu*

† Electronic supplementary information (ESI) available: Materials, instrumentation, synthetic procedures, supporting spectroscopic data. See DOI: 10.1039/d1sc06154b

study wavelength-dependent reactivity, we employed a wavelength-tuneable ns-pulsed laser system as a monochromatic light source to induce photoreactions at specific wavelengths, offering fine control over parameters such as wavelength, energy, and photon count.[30]

Results and discussion

Herein, we introduce a fully sequence-independent λ-orthogonal reaction system that solely relies on differences in absorption profiles and reaction quantum yields, without the need of altering reaction conditions, or using any kind of additive. We carefully probed the degree of λ-orthogonality at different wavelengths, using a combination of two UV and visible light activated photoactive molecules. Having identified the most suitable wavelengths, we employ a set of two appropriate LEDs to demonstrate the sequence-independence of the reaction system. As the UV-active component we chose a methoxy-substituted ***o*MBA**, which is well known to react cleanly and with high reaction quantum yield, forming a cycloadduct with *N*-(2-hydroxy)ethyl maleimide (Fig. 1, bottom left arrow).[32] As the visible light responsive component, we employed a recently developed red-shifted pyrene based tetrazole ((*N*,*N*-dimethyl)-aminopyrene aryl tetrazole, **APAT**) that is able to undergo NITEC reaction upon blue or green light irradiation (Fig. 1, top left arrow).[33] We hypothesized that **APAT** could be a suitable candidate for a sequence-independent λ-orthogonal system when combined with a shorter-wavelength photoreactive compound of higher quantum yield.

To determine reaction quantum yields for ***o*MBA** and **APAT**, small molecule ligation reactions were conducted in acetonitrile (MeCN), using *N*-(2-hydroxy)ethyl maleimide (***N*HEM**) as a ligation partner for both reactions. To obtain a complete picture, we chose a range of wavelengths (Fig. 2a). From previous studies, 320 nm and 450 nm were determined to be among the most efficient wavelengths for triggering the respective photoreactions.[32,33] 360 nm and 390 nm were chosen as intermediate wavelengths. The reaction products were analysed *via* liquid chromatography coupled with high-resolution mass spectrometry (LC-MS). ***o*MBA**, **APAT**, as well as their respective cycloadducts $\mathbf{CA}_{o\mathbf{MBA}}$ and $\mathbf{CA}_{\mathbf{APAT}}$ were quantified by correlating the integrals of the chromatogram peaks to the absorption coefficient $\varepsilon_{214\ \mathrm{nm}}$ of the respective species, where 214 nm is the scanning wavelength of the UV detector (refer to Fig. S1†). ***N*HEM** was used as a reaction partner because is it a common dipolarophile, and the hydroxy group provides sufficient separation of all involved species on the column, minimising peak overlap (Fig. 2b and c). Photo-induced NITEC yields pyrazoline-derivatives, which can undergo oxidation, forming aromatic pyrazoles. The degree of re-aromatization varies and is difficult to predict. While in most cases the irradiation experiments exclusively formed the pyrazole–cycloadduct, non-aromatic pyrazoline-species were observed as well (Fig. S2†). Attempts to isolate the cycloadduct led to the fully rearomatized pyrazole species. For analysis of the chromatograms, we therefore treated both species as one.

In Fig. 3, the photoreaction yield is plotted as a function of time. Since output energies were employed at different wavelengths, irradiation time is not the appropriate measure to compare the reaction kinetics. Instead, the top *x*-axis was adjusted to give the incident photon equivalents in relation to the number of chromophores in the solution. From Fig. 3a, it

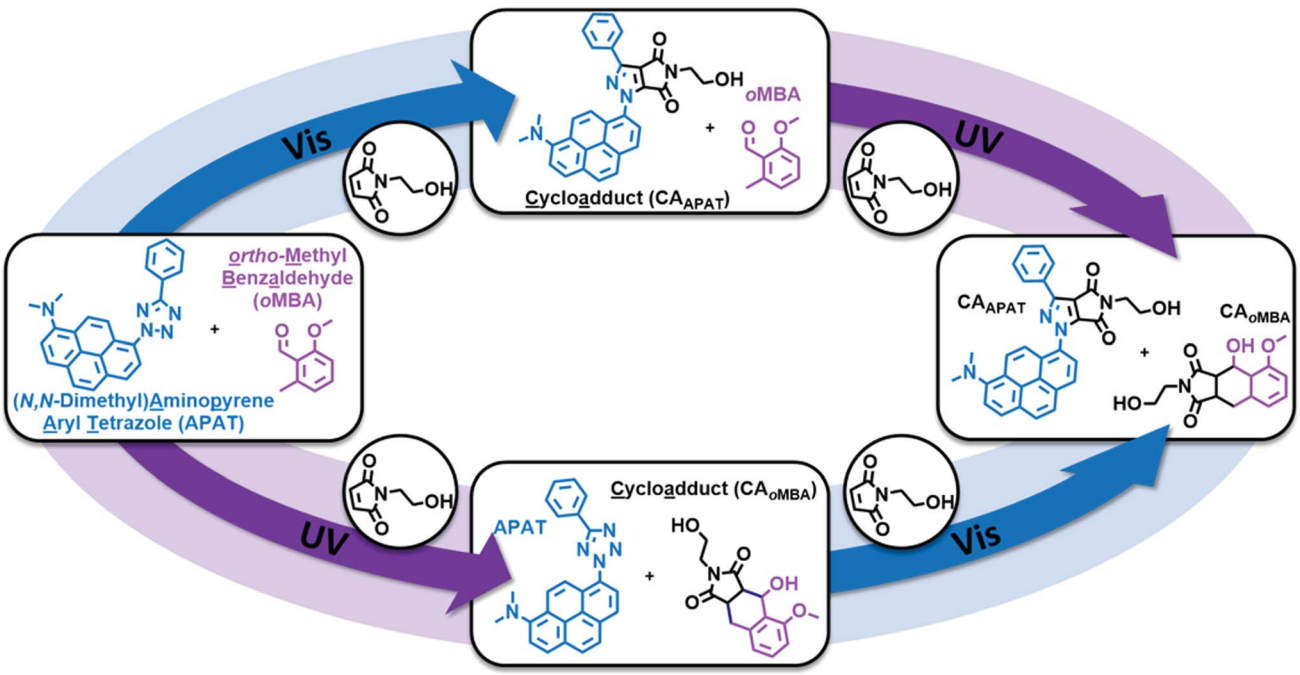

Fig. 1 Orthogonal photo-induced reactions of (*N*,*N*-dimethyl) aminopyrene aryl tetrazole (**APAT**) and *o*-methyl benzaldehyde (***o*MBA**) with *N*-(2-hydroxy)ethyl maleimide (***N*HEM**) in MeCN. Top left arrow: visible light activated nitrile imine-mediated tetrazole-ene cycloaddition (NITEC). Bottom left arrow: UV light activated *o*-quinodimethane-mediated Diels–Alder reaction of ***o*MBA**.

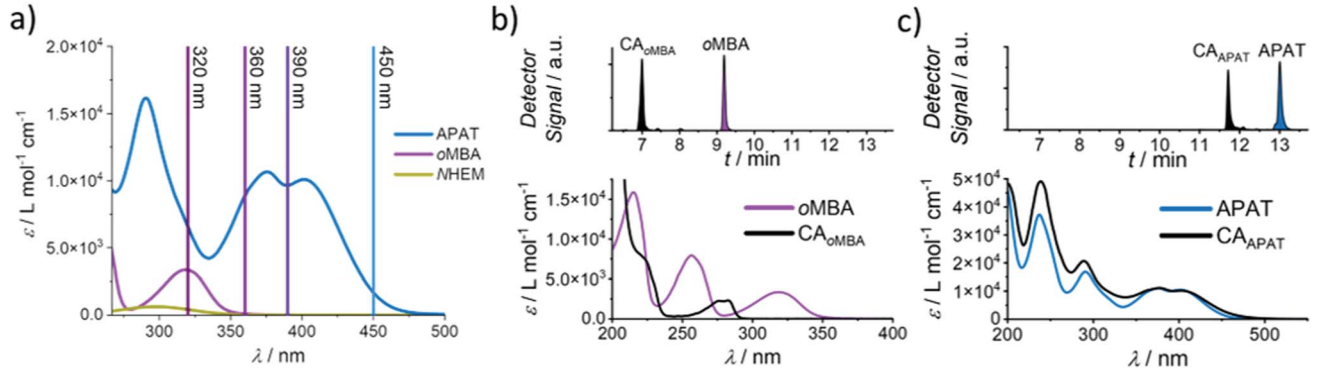

Fig. 2 (a) Absorption spectra of **APAT**, ***o*MBA** and ***N*HEM** in MeCN, as well as employed laser wavelengths. (b) (top) Chromatogram of ***o*MBA** and $\mathbf{CA}_{o\mathbf{MBA}}$ after 25 s at 320 nm irradiation. (bottom) Absorption spectra of ***o*MBA** (89 μM, in MeCN) and $\mathbf{CA}_{o\mathbf{MBA}}$ (49 μM, in MeCN/H_2O 92 : 8). (c) (top) Chromatogram of **APAT** and $\mathbf{CA}_{\mathbf{APAT}}$ after 30 min of 450 nm irradiation. (bottom) Absorption spectra of **APAT** (55 μM) and $\mathbf{CA}_{\mathbf{APAT}}$ (36 μM) in MeCN.

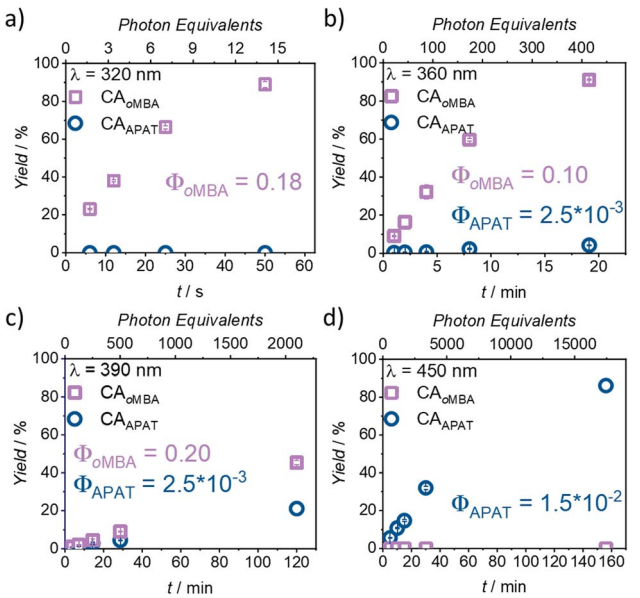

Fig. 3 Kinetic plots after irradiation with (a) 320 nm, (b) 360 nm, (c) 390 nm, and (d) 450 nm laser light. Photoreactions of ***o*MBA** (0.23 mM) and **APAT** (0.23 mM) with ***N*HEM** (1.82 mM) were carried out in degassed MeCN, and irradiation times were chosen to cover a wide range of conversions. Each experiment was repeated 3× to obtain error bars. Differences in the top and bottom *x*-axes stem from different laser energies and irradiation times. For detailed information, refer to ESI.†

becomes clear that ***o*MBA** and ***N*HEM** cleanly form the cycloadduct, yielding 89% after 50 s ($\Phi_{o\mathrm{MBA}} = 0.18 \pm 0.02$, for a detailed description of the determination of reaction quantum yields, refer to the ESI†). During this time, no detectable amounts of $\mathbf{CA}_{\mathbf{APAT}}$ are formed. We therefore assign a wavelength selectivity of at least 89% at 320 nm. The absorption coefficients of both compounds differ by a factor of two ($\varepsilon^{o\mathrm{MBA}}_{320\ \mathrm{nm}} = 3340 \pm 20$ L mol^{-1} cm^{-1}, $\varepsilon^{\mathrm{APAT}}_{320\ \mathrm{nm}} = 6570 \pm 30$ L mol^{-1} cm^{-1}), but due to the strongly disparate reaction quantum yields, ***o*MBA** reaches high conversion before **APAT** commences conversion. Similarly, ***N*HEM** in 8-fold excess acts as a competing chromophore ($\varepsilon^{\mathrm{NHEM}}_{320\ \mathrm{nm}} = 418 \pm 2$ L mol^{-1} cm^{-1}). At 360 nm irradiation (Fig. 3b), 91% yield of $\mathbf{CA}_{o\mathbf{MBA}}$ are reached after 19 min ($\Phi_{o\mathrm{MBA}} = 0.10 \pm 0.02$). We attribute the lower reactivity to two factors:

First, the absorptivity of ***o*MBA** at 360 nm is considerably lower ($\varepsilon^{o\mathrm{MBA}}_{360\ \mathrm{nm}} = 87 \pm 3$ L mol^{-1} cm^{-1}) compared to 320 nm. Secondly, the absorptivity of **APAT** ($\varepsilon^{\mathrm{APAT}}_{360\ \mathrm{nm}} = 8920 \pm 50$ L mol^{-1} cm^{-1}) is ∼90× higher. While ***o*MBA** alone at 360 nm retained approximately 60% of its reactivity at 320 nm in a previous study,[32] competing absorption of **APAT** further reduces the reactivity. Moreover, the reaction time is sufficiently long for **APAT** to reach 4% conversion ($\Phi_{\mathrm{APAT}} = (2.5 \pm 0.5) \times 10^{-3}$), lowering the overall degree of λ-orthogonality at this wavelength. Interestingly, in our initial study, **APAT** was close to six times more reactive at 320 nm (∼13% conversion) compared to 360 nm (∼2%).[33]

The same trend is observed at 390 nm (Fig. 3c). An even higher discrepancy between absorption coefficients and longer irradiation times led to rather similar conversions of both compounds after 120 min (45% $\mathbf{CA}_{o\mathbf{MBA}}$, $\Phi_{o\mathrm{MBA}} = 0.20 \pm 0.18$; 21% $\mathbf{CA}_{\mathbf{APAT}}$, $\Phi_{\mathrm{APAT}} = (2.5 \pm 0.5) \times 10^{-3}$). The large error in $\Phi_{o\mathrm{MBA}}$ stems from the uncertainty of $\varepsilon^{o\mathrm{MBA}}_{390\ \mathrm{nm}}$ (refer to ESI†). Finally, at 450 nm (Fig. 3d), no $\mathbf{CA}_{o\mathbf{MBA}}$ was detected even after 156 min of irradiation, while exclusively **APAT** was converted, yielding 86% of $\mathbf{CA}_{\mathbf{APAT}}$ ($\Phi_{\mathrm{APAT}} = (1.5 \pm 0.5) \times 10^{-2}$). We therefore assign a wavelength-selectivity of at least 86% at 450 nm. Clearly, of the investigated wavelengths, 390 nm is the least suitable for λ-orthogonality. This finding is especially interesting, because 390 nm is close to the absorption maxima of **APAT** (376 nm and 402 nm, respectively). Traditionally, wavelengths in λ-orthogonal reaction systems are determined by the absorption maxima of the involved chromophores. However, we herein show that 450 nm is the most appropriate wavelength, consistent with the reported findings of our preceding study on the reactivity of **APAT**. Yet, while our previous study reported increased reactivity at 320 nm,[33] herein, no conversion is observed within the reaction time of 50 s.

Having established the wavelengths with the highest selectivity (320 nm and 450 nm), we explored the λ-orthogonal

reaction system in a batch reaction, administering different colours of light in a defined sequence (refer to Fig. 4). The sequence includes both possible pathways (UV → vis, vis → UV) as well as a dark period. A 0.67 W LED, centred around 325 nm, was used to activate ***o*MBA**, while a 10 W LED, centred around 445 nm, was used to activate **APAT** (for emission spectra of the LEDs, refer to the ESI†).

We initially tested the UV → vis sequence, starting with the 325 nm LED. Although receiving significantly less photons per time unit due to the lower output power of the 325 nm LED, ***o*MBA** reacts close to five times faster than **APAT** due to the higher reaction quantum yield. Thus, samples were taken in 15 minute intervals. After a combined 45 min we found 60% yield for $\mathbf{CA}_{o\mathbf{MBA}}$, while no **APAT** cycloadduct was detected. After switching to a 445 nm 10 W LED, samples were taken every 40 min due to the longer reaction times required for **APAT**. To ensure that no thermal reaction was induced by the high-powered LED, we heated a solution of **APAT** and a dipolarophile in MeCN to 80 °C, yet found no change of the starting materials even after hours of heating (refer to ESI, Fig. S3†). After 120 min of irradiation (3 × 40 min) at 445 nm, a $\mathbf{CA}_{\mathbf{APAT}}$ yield of 35% was recorded, whereas the amount of $\mathbf{CA}_{o\mathbf{MBA}}$ remained constant. However, we found small amounts of side product (refer to ESI, Fig. S4†). We were not able to isolate the side product, however mass spectrometry indicates that it stems from the reaction between the nitrile imine and water (refer to Fig. S5†).[34] Repeated penetration of the rubber septum while withdrawing samples from the reaction mixture probably allowed small amounts of moisture to enter the reaction vessel. In the following 120 min dark period no increase in either of the species was observed. Subsequently, the vis → UV sequence was tested, starting with 445 nm irradiation. During visible light irradiation **APAT** continued to react and finally yielded 59% of $\mathbf{CA}_{\mathbf{APAT}}$ after another 120 min, while ***o*MBA** remained unaffected. Switching to 325 nm irradiation yielded a final 84% of $\mathbf{CA}_{o\mathbf{MBA}}$, with the amount of $\mathbf{CA}_{\mathbf{APAT}}$ remaining constant.

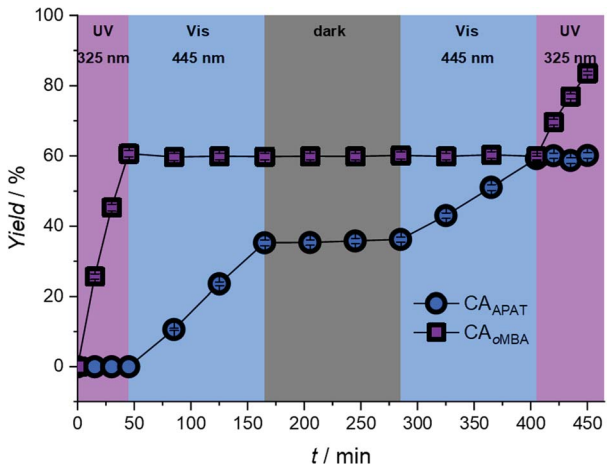

Fig. 4 Photoproduct yield of CA_{oMBA} and CA_{APAT} after sequential irradiation with two LEDs (325 nm, 0.67 W and 445 nm, 10 W), as well as a dark period. *o*MBA reacts exclusively upon 325 nm irradiation, while APAT only reacts to 445 nm light.

Conclusions

In summary, we introduce a fully sequence-independent λ-orthogonal reaction system, based on ***o*MBA** as a UV-activated photoactive moiety with high quantum yield, and **APAT** as a visible light activated unit with a low quantum yield. Initially, we probed the system at a range of specific wavelengths, using a tuneable ns-laser system, recording kinetic reaction plots, and determining the most suitable wavelengths for λ-orthogonality. Counterintuitively, 390 nm is the least suitable wavelength, despite being close to the absorption maxima of **APAT**. Instead, 450 nm led to exclusive conversion of **APAT**, whereas 320 nm addressed exclusively ***o*MBA**. Finally, we employed two spectrally broad LEDs (centred 325 nm and 445 nm) for sequential irradiation of both compounds within the reaction mixture, clearly demonstrating the individually addressable nature of the system. Our findings open an avenue for the construction of λ-orthogonal photoresists for 3D laser lithography.[35]

Data availability

Experimental data is available in the ESI.† Additional data is available upon request by contact with the corresponding author.

Author contributions

P. W. K. conducted the majority of all syntheses and the photochemical experiments. L. L. R. assisted with the syntheses as well as optimized and conducted the liquid chromatography experiments. S. L. W. conducted the quantum yield determination. A. N. U., J. P. B. and C. B.-K. conceptualized the study and were responsible for writing the grants on which the study is based (ARC Laureate C. B.-K., ARC Discovery C. B.-K. and J. P. B., KIT funding A. N. U.). All authors discussed the data and co-edited the manuscript.

Conflicts of interest

There are no conflicts to declare.

Acknowledgements

The authors thank Philipp Neidinger (Karlsruhe Institute of Technology) for the measurement of absorption spectra. C. B.-K. acknowledges funding by the Australian Research Council (ARC), in the context of a Laureate Fellowship underpinning his photochemical research program. C. B.-K. and J. P. B. acknowledge support *via* an ARC Discovery project targeted at red-shifting photoligation chemistry. Additional support by the Queensland University of Technology (QUT) and the Karlsruhe Institute of Technology (KIT) is gratefully acknowledged.

Notes and references

1 G. S. Kumar and Q. Lin, *Chem. Rev.*, 2020, **121**, 6991–7031.

2 K. Jung, N. Corrigan, M. Ciftci, J. Xu, S. E. Seo, C. J. Hawker and C. Boyer, *Adv. Mater.*, 2020, **32**, 1903850.
3 C. Brieke, F. Rohrbach, A. Gottschalk, G. Mayer and A. Heckel, *Angew. Chem., Int. Ed.*, 2012, **51**, 8446–8476.
4 M.-M. Russew and S. Hecht, *Adv. Mater.*, 2010, **22**, 3348–3360.
5 B. D. Fairbanks, L. J. Macdougall, S. Mavila, J. Sinha, B. E. Kirkpatrick, K. S. Anseth and C. N. Bowman, *Chem. Rev.*, 2021, **121**, 6915–6990.
6 J. J. Schwartz and A. J. Boydston, *Nat. Commun.*, 2019, **10**, 791.
7 N. D. Dolinski, Z. A. Page, E. B. Callaway, F. Eisenreich, R. V. Garcia, R. Chavez, D. P. Bothman, S. Hecht, F. W. Zok and C. J. Hawker, *Adv. Mater.*, 2018, **30**, 1800364.
8 K. Hiltebrandt, T. Pauloehrl, J. P. Blinco, K. Linkert, H. G. Börner and C. Barner-Kowollik, *Angew. Chem., Int. Ed.*, 2015, **54**, 2838–2843.
9 V. X. Truong, F. Li, F. Ercole and J. S. Forsythe, *ACS Macro Lett.*, 2018, **7**, 464–469.
10 P. Lu, D. Ahn, R. Yunis, L. Delafresnaye, N. Corrigan, C. Boyer, C. Barner-Kowollik and Z. A. Page, *Matter*, 2021, **4**, 2172–2229.
11 N. Corrigan, M. Ciftci, K. Jung and C. Boyer, *Angew. Chem., Int. Ed.*, 2021, **60**, 1748–1781.
12 C. G. Bochet, *Isr. J. Chem.*, 2021, **61**, 486–495.
13 A. Eibel, D. E. Fast, J. Sattelkow, M. Zalibera, J. Wang, A. Huber, G. Müller, D. Neshchadin, K. Dietliker, H. Plank, H. Grützmacher and G. Gescheidt, *Angew. Chem., Int. Ed.*, 2017, **56**, 14306–14309.
14 S. Bialas, L. Michalek, D. E. Marschner, T. Krappitz, M. Wegener, J. Blinco, E. Blasco, H. Frisch and C. Barner-Kowollik, *Adv. Mater.*, 2019, **31**, 1807288.
15 A. Ohtsuki, L. Lei, M. Tanishima, A. Goto and H. Kaji, *J. Am. Chem. Soc.*, 2015, **137**, 5610–5617.
16 S. Xu, J. Yeow and C. Boyer, *ACS Macro Lett.*, 2018, **7**, 1376–1382.
17 J. L. Pelloth, P. A. Tran, A. Walther, A. S. Goldmann, H. Frisch, V. X. Truong and C. Barner-Kowollik, *Adv. Mater.*, 2021, **33**, 2102184.
18 X. Zhang, L. Cox, Z. Wen, W. Xi, Y. Ding and C. N. Bowman, *Polymer*, 2018, **156**, 162–168.
19 M. Wu, X. Lin, X. Tan, J. Li, Z. Wei, D. Zhang, Y. Zheng, A.-X. Zheng, B. Zhao, Y. Zeng, X. Liu and J. Liu, *ACS Appl. Mater. Interfaces*, 2018, **10**, 19416–19427.
20 X. Zhang, W. Xi, S. Huang, K. Long and C. N. Bowman, *Macromolecules*, 2017, **50**, 5652–5660.
21 R. R. Batchelor, E. Blasco, K. N. R. Wuest, H. Lu, M. Wegener, C. Barner-Kowollik and M. H. Stenzel, *Chem. Commun.*, 2018, **54**, 2436–2439.
22 I. Elamri, C. Abdellaoui, J. K. Bains, K. F. Hohmann, S. L. Gande, E. Stirnal, J. Wachtveitl and H. Schwalbe, *J. Am. Chem. Soc.*, 2021, **143**, 10596–10603.
23 C. A. DeForest and K. S. Anseth, *Nat. Chem.*, 2011, **3**, 925–931.
24 J. A. Peterson, D. Yuan and A. H. Winter, *J. Org. Chem.*, 2021, **86**, 9781–9787.
25 W. A. Velema, J. P. van der Berg, W. Szymanski, A. J. M. Driessen and B. L. Feringa, *ACS Chem. Biol.*, 2014, **9**, 1969–1974.
26 C. G. Bochet, *Angew. Chem., Int. Ed.*, 2001, **40**, 2071–2073.
27 J. S. Clovis, A. Eckell, R. Huisgen and R. Sustmann, *Chem. Ber.*, 1967, **100**, 60–70.
28 J. P. Menzel, F. Feist, B. Tuten, T. Weil, J. P. Blinco and C. Barner-Kowollik, *Angew. Chem., Int. Ed.*, 2019, **58**, 7470–7474.
29 M. J. Hansen, W. A. Velema, M. M. Lerch, W. Szymanski and B. L. Feringa, *Chem. Soc. Rev.*, 2015, **44**, 3358–3377.
30 D. E. Fast, A. Lauer, J. P. Menzel, A.-M. Kelterer, G. Gescheidt and C. Barner-Kowollik, *Macromolecules*, 2017, **50**, 1815–1823.
31 D. E. Marschner, P. W. Kamm, H. Frisch, A.-N. Unterreiner and C. Barner-Kowollik, *Chem. Commun.*, 2020, **56**, 14043–14046.
32 J. P. Menzel, B. B. Noble, A. Lauer, M. L. Coote, J. P. Blinco and C. Barner-Kowollik, *J. Am. Chem. Soc.*, 2017, **139**, 15812–15820.
33 P. W. Kamm, J. P. Blinco, A.-N. Unterreiner and C. Barner-Kowollik, *Chem. Commun.*, 2021, **57**, 3991–3994.
34 S.-L. Zheng, Y. Wang, Z. Yu, Q. Lin and P. Coppens, *J. Am. Chem. Soc.*, 2009, **131**, 18036–18037.
35 L. Yang, F. Mayer, U. H. F. Bunz, E. Blasco and M. Wegener, *Light: Advanced Manufacturing*, 2021, **2**, 1–17.